Review of Scientific Instruments

Probing local electron temperature and density inside a sheared flow stabilized Z-pinch using portable optical Thomson scattering

Cite as: Rev. Sci. Instrum. **94**, 023508 (2023); https://doi.org/10.1063/5.0135265
Submitted: 17 November 2022 • Accepted: 30 January 2023 • Published Online: 17 February 2023

J. T. Banasek, C. Goyon, S. C. Bott-Suzuki, et al.

COLLECTIONS

F This paper was selected as Featured

SCI This paper was selected as Scilight

AIP Publishing

Review of Scientific Instruments | ARTICLE | scitation.org/journal/rsi

Probing local electron temperature and density inside a sheared flow stabilized Z-pinch using portable optical Thomson scattering

Cite as: Rev. Sci. Instrum. 94, 023508 (2023); doi: 10.1063/5.0135265
Submitted: 17 November 2022 • Accepted: 30 January 2023 •
Published Online: 17 February 2023

View Online Export Citation CrossMark

J. T. Banasek,[1,a)] C. Goyon,[2] S. C. Bott-Suzuki,[1] G. F. Swadling,[2] M. Quinley,[3] B. Levitt,[3] B. A. Nelson,[3] U. Shumlak,[3,4] and H. S. McLean[2]

AFFILIATIONS

[1] University of California San Diego, La Jolla, California 92093, USA
[2] Lawrence Livermore National Laboratory, 7000 East Avenue, Livermore, California 94550, USA
[3] Zap Energy, Seattle, Washington 98203, USA
[4] Aerospace and Energetics Research Program, University of Washington, Seattle, Washington 98195, USA

[a)] **Author to whom correspondence should be addressed:** jtbanas@sandia.gov

ABSTRACT

We report the first optical Thomson scattering measurements inside a high electron temperature ($\gtrsim$1 keV) and moderate electron density (mid 10^{16} cm^{-3}) plasma. This diagnostic has been built to provide critical plasma parameters, such as electron temperature and density, for Advanced Research Projects Agency-Energy-supported fusion-energy concepts. It uses an 8 J laser at 532 nm in 1.5 ns to measure the high frequency feature of the Thomson scattering profile at 17 locations along the probe axis. It is able to measure electron density from 5×10^{17} cm^{-3} to several 10^{19} cm^{-3} and electron temperatures from tens of eV to several keV. Here, we describe the design, deployment, and analysis on the sheared flow stabilized Z-pinch machine at Zap Energy named FuZE. The probe beam is aimed at an axial distance of 20 cm from the central electrode and is timed within the temporal envelope of neutron emission. The high temperature and moderate density plasmas generated on FuZE lie in an unconventional regime for Thomson scattering as they are between tokamaks and laser-produced plasmas. We described the analysis considerations in this regime, show that the electron density was below 5×10^{16} cm^{-3} at all times during these measurements, and present a sample shot where the inferred electron temperature varied from 167 ± 16 eV to 700 ± 85 eV over 1.6 cm.

I. INTRODUCTION

A key requirement to understand the evolution and dominant physical processes of plasma systems is the accurate diagnosis of plasma conditions. Quantifying both the magnitude and errors in experimentally measured parameters is vital, both where comparisons to simulation work are carried out and in the projection of plasma performance to new regimes, including the possibility of fusion energy.

Optical Thomson scattering, which refers to Thomson scattering in the ultraviolet, visible, or infrared wavelength domains, enables the local measurement of several plasma parameters, including electron density, electron temperature, and flow velocity. It has been deployed on many plasma research facilities spanning a wide range of electron densities, including laser produced plasmas,[1–3] pulsed power driven plasmas,[4–8] and tokamaks.[9] Thomson scattering provides quantitative measurements across these regimes, and work continues at both the high ($>1 \times 10^{18}$ cm^{-3}) and low ($<1 \times 10^{15}$ cm^{-3}) density range to extend the type of plasma conditions and parameters that can be studied by Thomson scattering.[10] Here, we present the design and analysis of a portable Thomson scattering diagnostic. It has been successfully deployed on the FuZE machine at Zap Energy, which operates a sheared-flow stabilized Z-pinch.[11] The expected parameters are mid density and high temperature, which creates a unique set of challenges compared to the traditional high- and low-density regimes used for Thomson scattering. In this density and temperature range, we were able to measure the electron temperature and find an upper bound on the electron density.

II. THOMSON SCATTERING THEORY

The non-collisional Thomson scattering profile is primarily defined by the Thomson scattering form factor[12]

$$S(\mathbf{k}, \omega) = \frac{2\pi}{k}\left|1 - \frac{\chi_e}{\epsilon}\right|^2 f_e\left(\frac{\omega}{k}\right) + \frac{2\pi Z}{k}\left|\frac{\chi_e}{\epsilon}\right|^2 f_i\left(\frac{\omega}{k}\right). \quad (1)$$

Here, $k = |\mathbf{k}_s - \mathbf{k}_l|$, with $\mathbf{k}_s$ and $\mathbf{k}_l$ being the scattering and laser wave-vectors, respectively, $\omega = \omega_s - \omega_l$, with ω_s and ω_l being the scattering and laser wave frequencies, respectively, Z is the ionization state, χ_e and χ_i are the electron and ion susceptibilities, respectively, $\epsilon = 1 + \chi_e + \chi_i$, and $f_e(v)$ and $f_i(v)$ are the electron and ion distribution functions, respectively. The form of the scattered spectrum is determined by the parameter $\alpha = 1/k\lambda_{De}$, where λ_{De} is the electron Debye length. In the case of alpha greater than one, the spectrum forms resonance peaks at the propagation velocity of the electron plasma wave (EPW) and ion acoustic wave (IAW). This condition is often referred to as the collective scattering limit. As alpha decreases below 1, the spectrum loses its peaked structure and begins to resemble the electron velocity distribution. This is often referred to as the non-collective limit of scattering. For a given scattering angle and laser wavelength, $\alpha \propto \sqrt{n_e/T_e}$, meaning that decreasing the electron density or increasing the electron temperature will make the scattering less collective.

For the case of collective scattering, the EPW, or high frequency feature, creates a pair of peaks that can be used to measure both the electron density, n_e, and electron temperature, T_e. In general, the density primarily drives the separation of the peaks, and the temperature drives the width of the peaks through Landau damping. While there is some correlation between these terms, they do make a unique fit to the scattered spectrum.

In the case of non-collective scattering, the spectral peaks disappear, resulting in a scattered profile that shows the electron distribution function. This enables the measurement of T_e from the width of the spectral profile. The total scattered intensity is proportional to the electron density, and, therefore, can be found by performing an absolute intensity calibration of the detector.

III. DESIGN CONSIDERATIONS FOR FUZE

This diagnostic was developed for the FuZE machine at Zap Energy.[11,13,14] The FuZE machine creates a sheared-flow stabilized Z-pinch form in a 50-cm long assembly region.[14] The arrangement for these experiments was made using an ignitron switched capacitor bank charged up to 25 kV and a pure deuterium gas fill. Inside the plasma column, thermonuclear reactions create a neutron line source.[15] In the shot described here, neutron production rises above the detection threshold starting at 17 μs into the experiment.

To develop the Thomson scattering system on FuZE, it is important to evaluate the desired measurements with the diagnostic, the estimated plasma conditions, and the location and formation of the plasma. For these experiments, the primary goal was the electron temperature, and the secondary goal was the electron density.

Expected plasma parameters can be estimated from previous experiments and scaling relations, and suggested densities near 1×10^{17} cm^{-3} and electron temperatures near 1 keV.[14] We use these parameters to calculate the scattering efficiency of the plasma and conduct photometric calculations to select a collection system and a laser that will have sufficient power to generate a measurable level of scattered photons on the detector. The maximum laser power and intensity is limited as it needs to remain low enough to not heat the plasma via inverse Bremsstrahlung,[16] nor filament within the plasma.[17]

In addition, these parameters are used to define a scattering angle for our system. Figure 1, showing synthetic Thomson scattering at various scattering angles, shows that even if the density is as high as 5×10^{17} cm^{-3}, collective scattering is only possible for scattering angles less than 15°. Collective scattering was desired to enable direct measurement of the electron temperature and density without needing to absolutely calibrate the intensity of the system. From the scaling of α, collective scattering would not be achieved for lower densities than this. We decided to adopt a scattering angle of 15° for two reasons. First it gave us the opportunity to see collective scattering if the density was at the upper end of the expected range. In addition, the small scattering angle enabled more collected scattering per pixel as the profile was narrower and the collection volume was larger compared to a larger scattering angle. A smaller angle than 15° was not possible due to the practical limitations in placing the output optics away from the laser exit.

Another way to increase α would be to go for longer wavelength Thomson scattering. This was initially considered by using a non-doubled 1064 nm laser. However, the efficiency of high-resolution detectors in the infrared region is significantly weaker than that in the visible. While using this laser wavelength could give a higher chance to achieve collective scattering, the loss of signal to noise makes the measurement too challenging.

Another design consideration arises from the formation of this plasma itself. Previous experiments showed the motion of the

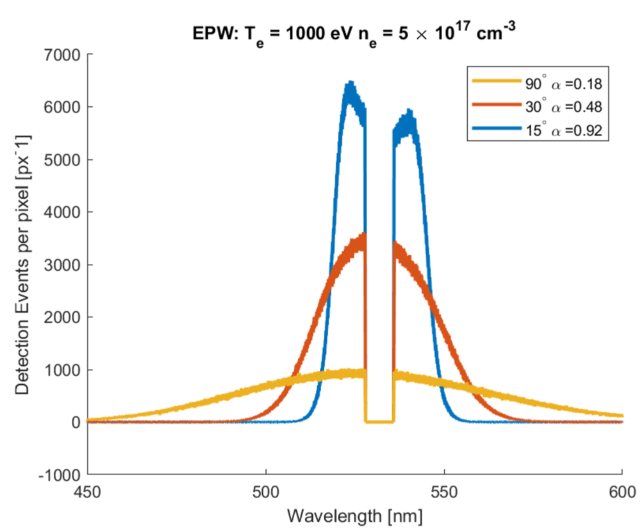

FIG. 1. Synthetic Thomson scattering spectra showing the effect of scattering angle on the shape of the profile for plasma with $n_e = 5 \times 10^{17}$ cm^{-3} and T_e = 1 keV. Going for a smaller angle causes the profile to become more collective. We see that at 15°, in blue, the spectrum begins to form the EPW peaks, which is the sign of collective scattering.

center-of-mass away from the central axis of the order 1 cm during the experiment, which makes observing the plasma column in each shot challenging.[11] By collecting from an extended spatial range along the laser path, we can be sensitive to variations in the plasma location in that direction. Since the plasma column size was expected to be 0.6 cm, we aimed for a field of view of 2 cm in order to be able to see a significant range of motion from the plasma along the laser direction.[18] While this design is not sensitive to motion perpendicular to the laser propagation direction and the plasma axis, we can use optical imaging to locate the plasma along this axis on every shot and correlate that to the Thomson scattering measurements. In addition, this machine has a relatively high shot rate— about one shot every 5 min—enabling a significant number of shots, to ensure we see the plasma column.

Other measurements with Thomson scattering, such as flow velocity and ion temperature, while not the primary focus, were still desired to be possible. These additional measurements would require observing the IAW feature, and, therefore, the capabilities to perform high resolution spectroscopy, <1 Å, were included in the design.

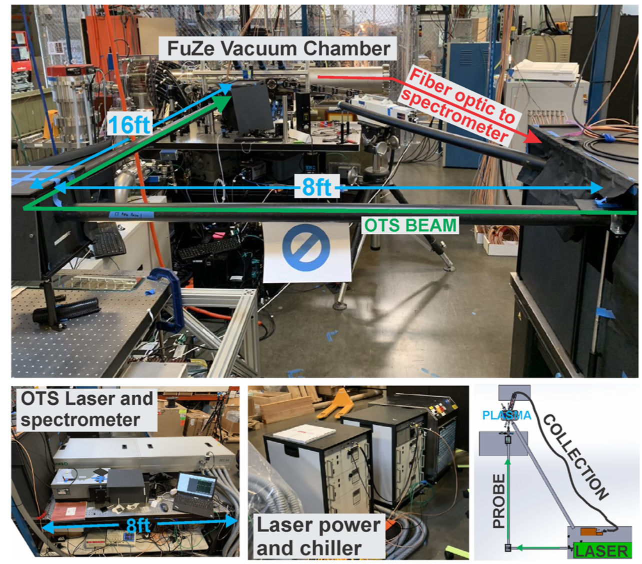

FIG. 2. Schematic and photographs of the optical Thomson scattering system deployed on the FuZE machine.

IV. EXPERIMENTAL ARRANGEMENT

A critical part of the Thomson scattering system is the laser. For this diagnostic, we used an Nd-YAG laser that was frequency doubled to produce 8 J of energy at 532 nm in 1.5 ns. Photometrics for the entire optical system discussed here show that with 8 J of laser energy, we should reach peak counts of 2000 photons per pixel at the estimated parameter range, which should provide a signal-to-noise ratio of 44 at the maximum gain of the camera. In addition, we verified that the laser energy is low enough that plasma heating or filamentation of the probe is not compromising the Thomson measurement. Assuming T_e of 1 keV, the energy deposited from the probe laser inside the plasma is negligible until the density is above 1×10^{21} cm^{-3}. Similarly, the threshold for beam filamentation is exceeded for $n_e > 2.5 \times 10^{19}$ cm^{-3}. Because the expected values for n_e are two orders of magnitude below the thresholds established for Te = 1 keV, we did not consider filamentation or plasma heating by the probe in the following analysis. If the plasma parameters were to approach these thresholds, we could lower the laser energy or intensity as necessary. The laser was focused to the center of the chamber using a 1000 mm focal length plano–convex lens placed outside of the vacuum chamber. The focal spot of the laser was ~250 μm as it was almost entirely blocked by a 200 μm diameter pin. This laser and its path to the FuZE chamber are shown in Fig. 2.

In order to collect the scattered radiation from the plasma, a linear fiber bundle was used. This enabled easy delivery of the scattered light from the plasma to the spectrometer/imaging system and allowed flexibility in its location. It also enabled flexibility in the design of the collection volume and resolution along the laser direction. The fiber bundle used for this experiment was a linear array of 27 fibers—each with a diameter of 100 μm, center to center spacing of 130 μm, and a numerical aperture of 0.12, or f/4. The spectrometer side of the fiber bundle had a center-to-center separation of 390 μm. This larger separation was used to ensure that each fiber could be individually resolved on the detector. The low numerical aperture was selected in order to better match the f-number of the spectrometer, f/6. Of the 27 fibers, only 17 were viewable on the detector due to the magnification into the spectrometer. In the future iterations, if some light could be sacrificed, it would be possible to observe more fibers on the detector by changing the coupling optics in the spectrometer.

To collect light from the experiment and deliver it to the fiber bundle, a pair of achromatic doublets were used. Both doublets were 2 in. in diameter and had focal lengths of 400 and 200 mm. This resulted in a two times magnification of the fibers at the center of the chamber. With the 15° scattering angle, the system had a full width at half maximum (FWHM) of 0.74 mm for the fiber field of view and a 1.0 mm fiber center-to-center separation. Each fiber, therefore, has a collection volume of $0.25 \times 0.25 \times 0.74$ mm^3, and the total field of view for all 17 fibers is 16 mm, which was close to our goal of 2 cm and enables detecting motion of the plasma along the laser's axis. This lens assembly and the fiber bundle were mounted outside of the vacuum chamber to collect light from the plasma.

In order to couple the light from the fiber bundle into the spectrometer, another optical relay was used, as shown in green in Fig. 3. This relay was used to both improve the amount of light entering the spectrometer by matching the f-number and to give a collimated region, to put other optics such as notch filters or beam splitters. One important consideration with this relay design was the reduction of off-axis losses through the relay as the active part of the fiber bundle had a length of 6.6 mm, which can lead to large off-axis effects. In order to correct for these effects, the collecting lens was a 1″ diameter achromatic doublet with a 75 mm focal length, while the focusing lens was a 2″ diameter achromatic doublet with a 150 mm focal length, and they were separated by 250 mm. The collecting lens had a smaller f-number than the fiber bundle in order to fully collect the light from each fiber. The separation between the lens and the large diameter of the second lens is to correct for the off-axis tilt and

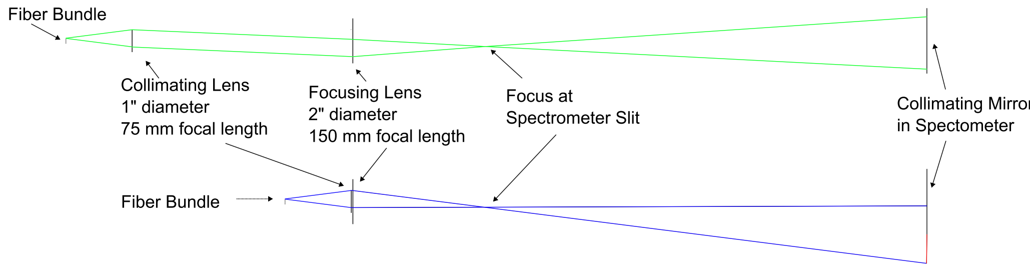

FIG. 3. Diagram of the optical relay for coupling from the fiber bundle into the spectrometer. In green (top), we show the extreme rays from the edge fiber with 250 mm separation between the lenses, while in blue (bottom), we show the rays if there was no separation. We see that all the rays from the edge fiber reach the collimating mirror in the spectrometer with the separation, but not when the lenses are right next to each other (lost region shown in red at the bottom right).

allow the edge fibers to be well coupled through the spectrometer, as shown in Fig. 3. This design enabled 100% of the light from the edge fibers to reach the detector, instead of 50%, if a simple f-matched relay were to be used.

The spectrometer and the detector were the Andor 500 mm Shamrock Czerny–Turner spectrometer and the Andor iStar CMOS detector, respectively. The 500 mm focal length spectrometer was used in order to give flexibility in the design to detect both the IAW and EPW features. With a low-resolution grating, 150 L/mm, the spectrometer would have the bandwidth to observe the EPW feature, while with a highresolution grating, 2400 L/mm, the IAW could be resolved. As we were focused on the EPW, the 150 L/mm grating was used in these experiments. The CMOS camera had a minimum gate width of 1.5 ns. While keeping the gate width small is desirable, as it helps reduce parasitic laser radiation and continuum radiation, the gate width was set to 4 ns. This was chosen, as we observed a significant Thomson signal increase during experiments compared to a 2 ns gate, while continuum radiation and parasitic light were still minimal. This increase in the Thomson scattered signal could be due to slight inaccuracies in the timing, timing jitter, possible underestimates of the gate width at its minimal setting, or inefficiencies or non-linearity in the gain of the camera at short exposure lengths.

In order to mount the laser delivery and Thomson scattering collection optics onto the chamber, three flanges needed to be designed. These were the input flange, output flange, and the top flange, as shown in Fig. 4. The side flanges enabled accurate mounting of the diagnostic to the chamber while providing some standoff

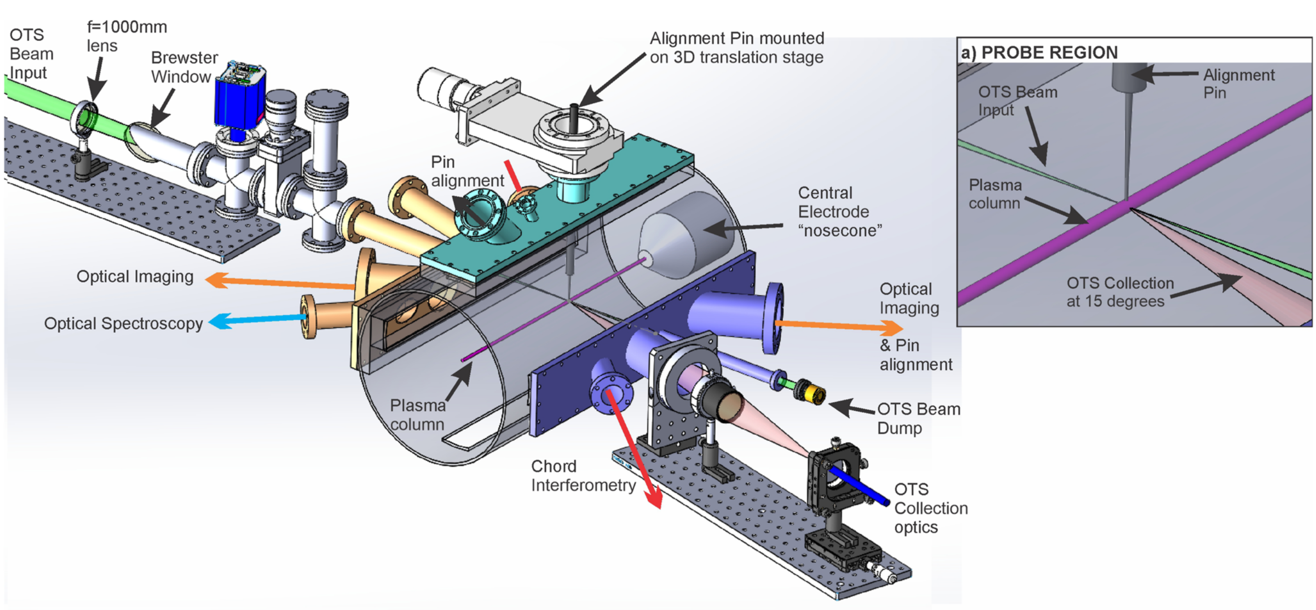

FIG. 4. Three flanges designed for use on the FuZE chamber. They allow for both flexible Thomson scattering setups, as well as multiple line of sight diagnostics to be used with them, all looking at P20. The input flange is orange, the output flange is purple, and the top flange is green.

from the plasma to reduce debris on the windows. The top flange was used to enable the mounting of a vacuum translation stage, which was used to place a pin in the center of the chamber, enabling alignment of the fiber bundle and the Thomson scattering laser while under vacuum. This alignment was performed by lowering a 200 μm diameter needle into the center of the chamber. The scattered intensity from the pin was then maximized into the fiber bundle, by adjusting the position of the fibers, demonstrating that the fiber and laser are accurately aligned. Additional ports were placed on the flange to both provide access for other diagnostics on the FuZE chamber and provide options for scattering at other angles. In addition, while shown here for collection at 20 cm away from the nose cone (P20), the diagnostic could be completely inverted, enabling collection at 28 cm from the nose cone.

The Thomson scattering design also included the possibility of transporting the whole system for deployment on other fusion devices after this initial demonstration. While Thomson scattering is rather involved and requires specific access to the plasma, as discussed above, some considerations can be made to simplify the transport and setup for the major components. The laser head, spectrometer and CMOS, and a laptop to control the system and acquire data are all mounted on a single 8' × 4' optical table, as shown in Fig. 2. Initial beam delivery optics as well as fiber collection and focus into the spectrometer are also mounted here. Both this table and the power supply and chiller units are mounted on wheeled chassis to allow easy transport and positioning of the system in the laboratory. These can be located relative to the experiment, accounting for exclusion zones for electromagnetic interference or radiation, and then the remaining beam delivery and collection optics for a specific experiment can be put in place. Once suitable vacuum chamber modifications and laser safety procedures are completed, the system typically takes one week to set up, for full operation and data collection.

A typical design challenge in Thomson scattering systems is the presence of parasitic (or stray) laser radiation. However, it is difficult to predict, as it depends greatly on the details of the specific experiment. Here, we observed a significant amount of stray laser radiation, likely from the laser interacting with the walls of the chamber, or the entrance and exit tubes. While the short gate width was picked to hopefully reduce the stray light, initial experiments showed that the laser light was too strong to observe the EPW scattering feature. Therefore, we included a notch filter in order to block the stray laser light. While this filter was centered near the laser wavelength, at 533 nm, it had a FWHM of 17 nm. This would cause the notch filter to block the entirety of the EPW feature for lower density and temperature plasma. The notch filter was set at an angle of 18° to shift the central wavelength, aligning the filter transmission cut-off to the observed edge of the laser line. This enabled the maximum collection of the red shifted EPW feature, while preventing the stray laser light from entering the system. The effect of the shifted notch filter on the spectrum is shown in Fig. 5.

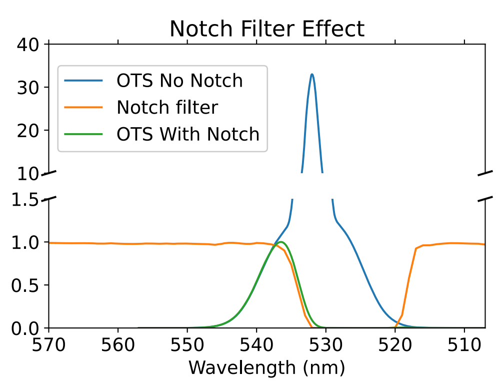

FIG. 5. The spectrum with the stray laser light being 30 times stronger than the Thomson scattering signal is shown in blue, with $n_e = 1 \times 10^{17}$ cm^{-3} and $T_e = 500$ eV. We see that the EPW feature is very weak and could not be detected. By setting the notch filter (orange) as shown, we can detect and measure the Thomson scattering signal(green).

V. CALIBRATION

In order to properly analyze the data, several calibrations needed to be performed. These calibrations included defining the dispersion of the spectrometer, the location of the laser wavelength, the instrumental response function, the intensity as a function of wavelength, and the location of the notch filter.

The first calibration was a wavelength calibration, which enabled finding the spectrometer dispersion and the location of the laser. This was performed using a Ne calibration lamp and the spectral lines at 621.7, 594.5, 576.4, and 540.1 nm. This gives a measurement of the dispersion for the entire spectrometer; however, if there is a slight rotation of the fiber bundle relative to the slit, it would cause a slight shift in the spectrum between each fiber. In order to correct for this shift, a spectrum was taken without the notch filter to collect the stray laser light on each fiber. This results in the laser on each individual fiber, which allows us to perform a linear shift of the spectrum for each individual fiber based on the wavelength of the laser.

The shot with stray laser light was also used to find the instrumental response function. The laser light allows us to find the instrumental profile for each fiber because of the narrow bandwidth of the probe laser. The instrumental function was assumed to be a Gaussian profile, and the FWHM of the profile was fitted to be near 2.1 nm. The fit and estimated error for a single fiber is shown in Fig. 6.

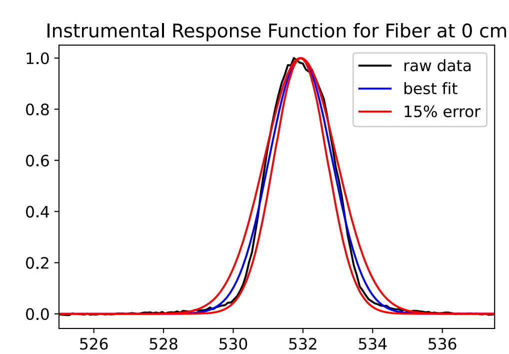

FIG. 6. Best fit to the instrumental function for the fiber at the center of the chamber. The FWHM of the Gaussian was 2.1 nm. The red traces show the 15% error that was used for the Monte Carlo error calculations discussed later.

A relative intensity calibration was also performed, which accounts for the optics and detector having different sensitivities at different wavelengths. First, a background subtraction was performed to ensure a flat baseline. Then, a halogen white light source with a known relative emission spectrum was shone through the fiber bundle. A fit between that spectrum and the collected data, with differences being able to be modeled as an intensity scaling factor to correct the raw data, was obtained.

The final calibration was the spectral wavelengths rejected by the notch filter for each fiber. This was done by shining the white light through the system with the notch filter installed. It was then possible to observe the spectral location of the notch filter on each individual fiber. Combining lineouts of each of these fibers with the specifications for the notch filter enables determination of the shift in the central wavelength value of the notch filter for each fiber. This shift and the notch filter specifications can then be applied to the raw data for each individual fiber.

VI. DATA

To demonstrate the capabilities of this diagnostic to measure a range of electron temperatures, we will show the analysis for a shot with a strong gradient in the electron temperature over the fibers. Data for our experiments were gathered at various times with respect to the neutron emission to measure the changing plasma conditions. The raw data from shot number 220609021 is shown in Fig. 7 and was gathered at 470 ns after the start of the neutron pulse. Each of the lines is a different radial location within the plasma. Looking from the bottom to the top of the image, we see a significant change in the width of the spectrum, which denotes a higher electron temperature for the fibers at the bottom of the image compared to those near the top of the image. However, we do not see distinct peaks in the spectrum, meaning we are not in the collective regime, and, therefore, cannot make a direct measurement of the electron density without an absolute calibration of our system.

Though we do not have an absolute intensity calibration of the system, we can still look at both—relative intensities between all shots and some of the fits—to get an idea of the electron density and improve our measurements of T_e. By using the fits to the low temperature (<200 eV) Thomson scattering results, we can find an upper bound on the density. Figure 8 shows fits to the lowest temperature fiber from shot 220609021 using two fixed densities. We see that as density goes above 5×10^{16} cm^{-3}, it becomes impossible to fit the edge of the spectrum created by the notch filter. This shift from the notch edge at higher densities is a result of the spectrum changing shape and moving away from the non-collective spectrum. Since we see this in all of the low temperature shots, we make the assumption that in the low temperature cases, the density is less than 5×10^{16} cm^{-3}.

Now, we can look at the intensity of the signal as the signal broadens, indicating an increase in temperature. In the non-collective regime, the total scattered intensity scales linearly with density.[12] In addition, for our notch filter location, the maximum intensity for a given density varies by only 50% over the temperature range between 100 and 3000 eV, with a maximum value at 450 eV. If we look at the number of counts as a function of fitting temperature, Fig. 9, we see that the maximum number of counts is decreasing as the temperature of the fit increases. Since this decrease is significantly more than the 50% variation for a given density and counts increase with increasing density, this shows that the higher temperature shots must be at a lower density than the low temperature shots. As already discussed, the low temperature shots must be below densities of 5×10^{16} cm^{-3}. This intensity trend means that this density can then be used as an upper bound for all shots. This decrease in density with increasing temperature is also consistent with the assumption of pressure balance within the plasma.

As density decreases, so does α, meaning that the scattering becomes more non-collective. Eventually, the density will no longer influence the electron temperature, and, therefore, we can set a lower bound for the fitting density. For example, fitting the bottom fiber in

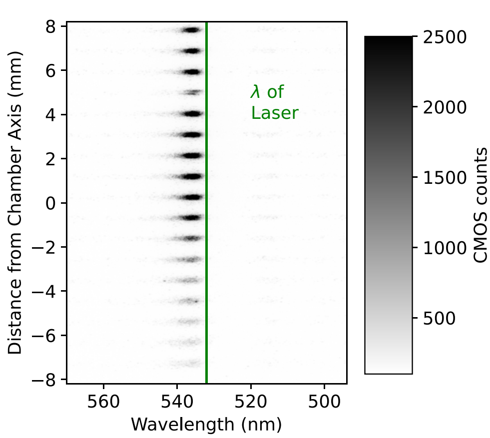

FIG. 7. Raw data for shot 220609021. The shot shows a range of different temperatures due to the changes in the width of the spectrum. These data were gathered at 470 ns in the neutron pulse.

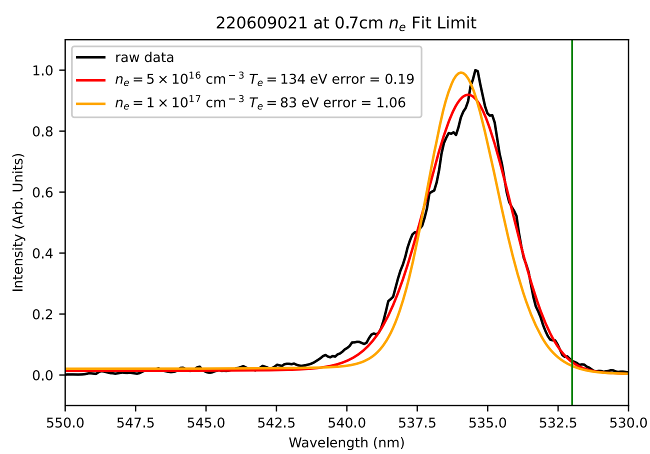

FIG. 8. Best fit for the coldest fiber for shot 220609021. Green line is the laser line, black is the raw data, red is the best fit at $n_e = 5 \times 10^{16}$ cm^{-3}, and orange is the best fit at $n_e = 1 \times 10^{17}$ cm^{-3}. We see here that the higher density trace clearly cannot fit the edge of the notch filter (right edge of the profile), and, therefore, is too high of a density for this fit.

Fig. 7 would result in T_e = 633 eV for 5 × 10^{16} cm^{-3}, T_e = 742 eV for 5 × 10^{15} cm^{-3}, and T_e = 755 eV for 1 × 10^{14} cm^{-3}. As we see little change in T_e between 5 × 10^{15} and 1 × 10^{14} cm^{-3}, we can safely use n_e = 5 × 10^{15} cm^{-3} as a lower bound for our fits.

The data now can be fit by a non-collisional Thomson scattering model. The model had three parameters—T_e, peak intensity, and continuum intensity. The continuum intensity was a vertical shift of the profile to account for the counts in the continuum of the spectrum. We then performed fits at the upper and lower bounds of our density range to find a range for the electron temperature. Though velocity can create a Doppler shift in the collected spectrum, due to our choice of scattering angle, a velocity of 200 km/s, the maximum found on previous experiments,[11] would result in only a shift of 0.9 Å and, therefore, can safely be ignored.

Error bars were found using a Monte Carlo error technique of 1000 different fits.[2] The parameters that were allowed to vary were the width of the instrumental function, by 15%, the accuracy of the laser wavelength, by 1 nm, and the dispersion of the spectrometer, by 1.5%. For each fit, noise was added to the theoretical profile before performing the fit. This noise, σ, was modeled as a basic Poisson noise with camera noise added[19]

$$\sigma^2 = yG + n\sigma_{pix}^2, \tag{2}$$

with y being the number of counts for that wavelength, G = 1000 was the gain of the CMOS camera, n was the number of rows used to create the lineout, and σ_{pix} was the noise in the camera with no signal and was equal to 11. In addition, fits were performed at both 5 × 10^{15} and 5 × 10^{16} cm^{-3}, as those were the bounds discussed above. The reported value for T_e is the average of these two fits, with the error bars being the sum in quadrature of the error of the two different fits.

The best fit and error bars for several of the fibers are shown in Fig. 10, and the electron temperature of all of the fibers for this shot is shown in Fig. 11. We see that for this shot, the plasma increases in temperature from one side to the other, going from 167 ± 16 eV up to 700 ± 85 eV. Seeing these changes in the scattering profile within a single shot and how T_e changes because of these fits helps give us confidence in the accuracy of our fits and that we can make useable measurements of the plasma conditions.

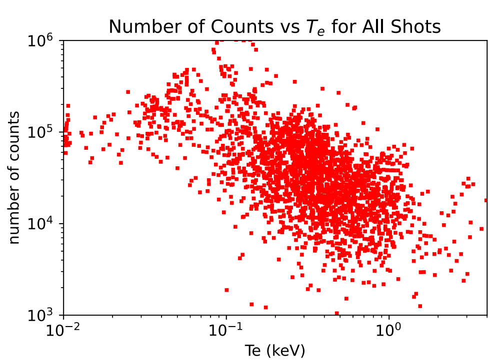

FIG. 9. Number of counts as a function of the best fit electron temperature, assuming that n_e = 5 × 10^{16} cm^{-3} for all fit. As T_e increases, the number of counts in the peaks decreases, suggesting that n_e is decreasing at higher temperatures.

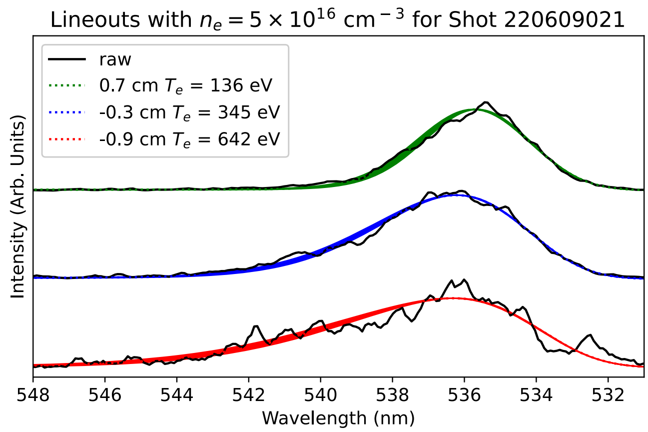

FIG. 10. Best fits for several fibers for shot 220609021, assuming that the density is n_e = 5 × 10^{16} cm^{-3}. The raw data are in black, best fits are the dotted lines, and 1σ errors from the Monte Carlo calculations for this density are the shaded regions.

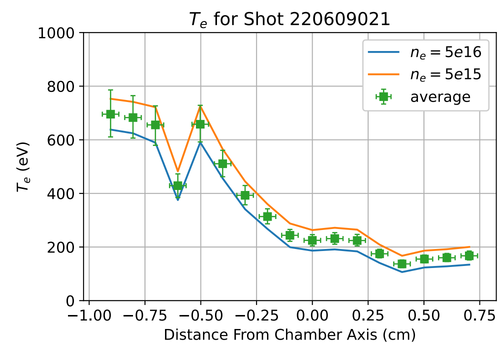

FIG. 11. Measured T_e for shot 220609021. Blue line is the fit at n_e = 5 × 10^{16} cm^{-3}, orange line is the fit at n_e = 5 × 10^{15} cm^{-3}, and the green points are the average of those two fits, with the error bars based on the Monte Carlo error calculations for the two fits. The horizontal error bars are the FWHM of each fiber.

VII. CONCLUSION

In this paper, we have described the design, implementation, and analysis techniques for an optical Thomson scattering system on the sheared-flow stabilized Z-pinch on the FuZE machine. It is the first optical Thomson scattering measurement inside a high electron temperature (≳1 keV) and moderate electron density (mid 10^{16} cm^{-3}) plasma. The use of a fiber bundle in the collection system leads to 17 distinct measurement locations along the laser axis, providing a 1.6 cm field of view. The design relies on a small scattering angle to maximize the scattered signal and lower the density required in the collective scattering regime. We show that $n_e \leq 5 \times 10^{16}$ cm^{-3} using the magnitude of the scattered signal. It allows us to infer the electron temperature with a 10% accuracy. In addition, we detail the analysis performed on one shot, with temperatures ranging from 167 ± 16 eV up to 700 ± 85 eV across our field of view.

These measurements show that the Thomson scattering diagnostic can make detailed measurements of at least T_e and possibly n_e in plasmas generated on FuZE. These measurements will be able to be compared to other diagnostics, such as the neutron production rate, to gain a better understanding of the plasma. Going forward, this diagnostic will be able to probe other locations of the FuZE plasma column and, with a reduction of stray light, could observe the IAW spectral feature. Finally, our Thomson scattering detector includes the possibility of transporting the system for deployment on other fusion devices after this initial demonstration. It is able to measure electron density from $n_e \sim 5 \times 10^{17}$ cm^{-3} to several 10^{19} cm^{-3} and temperatures from tens of eV to several keV, which is a range of interest for the high energy density plasma community.

ACKNOWLEDGMENTS

C. Goyon would like to thank G. Wurden and J. A. Angus for fruitful discussions on the sheared-flow stabilized plasma behavior. The information, data, and work presented herein were funded in part by the Advanced Research Projects Agency-Energy (ARPA-E), U.S. Department of Energy, under Award Nos. DE-AR0001165, DE-AR-0000571, DE-AR-0001010, and DE-AR-0001260, and prepared by LLNL, under Contract No. DE-AC52-07NA27344. The views and opinions of the authors expressed herein do not necessarily state or reflect those of the United States Government, nor any agency thereof (LLNL-JRNL-840928).

AUTHOR DECLARATIONS

Conflict of Interest

The authors have no conflicts to disclose.

Author Contributions

J. T. Banasek: Conceptualization (equal); Formal analysis (equal); Investigation (equal); Methodology (equal); Software (lead); Writing – original draft (lead); Writing – review & editing (equal). **C. Goyon**: Conceptualization (equal); Formal analysis (equal); Funding acquisition (lead); Investigation (equal); Methodology (equal); Project administration (lead); Supervision (equal); Writing – original draft (supporting); Writing – review & editing (equal). **S. C. Bott-Suzuki**: Conceptualization (equal); Formal analysis (equal); Investigation (equal); Methodology (equal); Supervision (equal); Writing – original draft (supporting); Writing – review & editing (equal). **G. F. Swadling**: Formal analysis (supporting); Investigation (supporting); Methodology (supporting); Writing – review & editing (equal). **M. Quinley**: Methodology (supporting); Resources (supporting); Writing – review & editing (equal). **B. Levitt**: Investigation (supporting); Resources (equal); Writing – review & editing (equal). **B. A. Nelson**: Investigation (supporting); Resources (equal); Writing – review & editing (equal). **U. Shumlak**: Investigation (supporting); Resources (equal); Writing – review & editing (equal). **H. S. McLean**: Funding acquisition (equal); Supervision (equal); Writing – review & editing (equal).

DATA AVAILABILITY

The data that support the findings of this study are available from the corresponding author upon reasonable request.

REFERENCES

[1] J. S. Ross, S. H. Glenzer, J. P. Palastro, B. B. Pollock, D. Price, L. Divol, G. R. Tynan, and D. H. Froula, "Observation of relativistic effects in collective Thomson scattering," Phys. Rev. Lett. **104**, 105001 (2010).

[2] R. K. Follett, J. A. Delettrez, D. H. Edgell, R. J. Henchen, J. Katz, J. F. Myatt, and D. H. Froula, "Plasma characterization using ultraviolet Thomson scattering from ion-acoustic and electron plasma waves (invited)," Rev. Sci. Instrum. **87**, 11E401 (2016).

[3] J. S. Ross, P. Datte, L. Divol, J. Galbraith, D. H. Froula, S. H. Glenzer, B. Hatch, J. Katz, J. Kilkenny, O. Landen, A. M. Manuel, W. Molander, D. S. Montgomery, J. D. Moody, G. Swadling, and J. Weaver, "Simulated performance of the optical Thomson scattering diagnostic designed for the national ignition facility," Rev. Sci. Instrum. **87**, 11E510 (2016).

[4] J. T. Banasek, S. V. R. Rocco, W. M. Potter, T. Byvank, B. R. Kusse, and D. A. Hammer, "Multi-angle multi-pulse time-resolved Thomson scattering on laboratory plasma jets," Rev. Sci. Instrum. **89**, 10C109 (2018).

[5] G. F. Swadling, S. V. Lebedev, A. J. Harvey-Thompson, W. Rozmus, G. C. Burdiak, L. Suttle, S. Patankar, R. A. Smith, M. Bennett, G. N. Hall, F. Suzuki-Vidal, and J. Yuan, "Interpenetration, deflection, and stagnation of cylindrically convergent magnetized supersonic tungsten plasma flows." Phys. Rev. Lett. **113**, 035003 (2014).

[6] G. F. Swadling, S. V. Lebedev, G. N. Hall, S. Patankar, N. H. Stewart, R. A. Smith, A. J. Harvey-Thompson, G. C. Burdiak, P. de Grouchy, J. Skidmore, L. Suttle, F. Suzuki-Vidal, S. N. Bland, K. H. Kwek, L. Pickworth, M. Bennett, J. D. Hare, W. Rozmus, and J. Yuan, "Diagnosing collisions of magnetized, high energy density plasma flows using a combination of collective Thomson scattering, Faraday rotation, and interferometry (invited)," Rev. Sci. Instrum. **85**, 11E502 (2014).

[7] T. Byvank, J. T. Banasek, W. M. Potter, J. B. Greenly, C. E. Seyler, and B. R. Kusse, "Applied axial magnetic field effects on laboratory plasma jets: Density hollowing, field compression, and azimuthal rotation," Phys. Plasmas **24**, 122701 (2017).

[8] J. D. Hare, J. MacDonald, S. Bland, J. Dranczewski, J. Halliday, S. V. Lebedev, L. Suttle, E. Tubman, and W. Rozmus, "Two-colour interferometry and Thomson scattering measurements of a plasma gun," Plasma Phys. Controlled Fusion **61**, 085012 (2019).

[9] N. J. Peacock, D. C. Robinson, M. J. Forrest, P. D. Wilcock, and V. V. Sannikov, "Measurement of the electron temperature by Thomson scattering in tokamak T3," Nature **224**, 488–490 (1969).

[10] A. L. Milder, J. Katz, R. Boni, J. P. Palastro, M. Sherlock, W. Rozmus, and D. H. Froula, "Statistical analysis of non-Maxwellian electron distribution functions measured with angularly resolved Thomson scattering," Phys. Plasmas **28**, 082102 (2021).

[11] A. D. Stepanov, U. Shumlak, H. S. McLean, B. A. Nelson, E. L. Claveau, E. G. Forbes, T. R. Weber, and Y. Zhang, "Flow Z-pinch plasma production on the FuZE experiment," Phys. Plasmas **27**, 112503 (2020).

[12] D. Froula, S. H. Glenzer, N. C. J. Luhmann, and J. Sheffield, *Plasma Scattering of Electromagnetic Radiation: Theory and Measurement Techniques*, 2nd ed. (Elsevier, Amsterdam, 2011), p. 520.

[13] Y. Zhang, U. Shumlak, B. A. Nelson, R. P. Golingo, T. R. Weber, A. D. Stepanov, E. L. Claveau, E. G. Forbes, Z. T. Draper, J. M. Mitrani, H. S. McLean, K. K. Tummel, D. P. Higginson, and C. M. Cooper, "Sustained neutron production from a sheared-flow stabilized Z pinch," Phys. Rev. Lett. **122**, 135001 (2019).

[14]U. Shumlak, "Z-pinch fusion," J. Appl. Phys. **127**, 200901 (2020).
[15]J. M. Mitrani, D. P. Higginson, Z. T. Draper, J. Morrell, L. A. Bernstein, E. L. Claveau, C. M. Cooper, E. G. Forbes, R. P. Golingo, B. A. Nelson, A. E. Schmidt, A. D. Stepanov, T. R. Weber, Y. Zhang, H. S. McLean, and U. Shumlak, "Measurements of temporally- and spatially-resolved neutron production in a sheared-flow stabilized Z-pinch," Nucl. Instrum. Methods Phys. Res., Sect. A **947**, 162764 (2019).
[16]J. T. Banasek, T. Byvank, S. V. R. Rocco, W. M. Potter, B. R. Kusse, and D. A. Hammer, "Time-resolved thomson scattering on laboratory plasma jets," IEEE Trans. Plasma Sci. **46**, 3901–3905 (2018).
[17]A. M. Hansen, D. Turnbull, J. Katz, and D. H. Froula, "Mitigation of self-focusing in Thomson scattering experiments," Phys. Plasmas **26**, 103110 (2019).
[18]H. Zhao, Z. Li, D. Yang, X. Li, Y. Chen, X. Jiang, Y. Liu, T. Gong, L. Guo, S. Li, Q. Li, F. Wang, S. Liu, J. Yang, S. Jiang, W. Zheng, B. Zhang, and Y. Ding, "Progress in optical Thomson scattering diagnostics for ICF gas-filled hohlraums," Matter Radiat. Extremes **4**, 055201 (2019).
[19]G. F. Swadling, C. Bruulsema, W. Rozmus, and J. Katz, "Quantitative assessment of fitting errors associated with streak camera noise in Thomson scattering data analysis," Rev. Sci. Instrum. **93**, 043503 (2022).